

Cluster Bose Metals

Tao Ying,^{1,2,3} Marcello Dalmonte,⁴ Peter Zoller,⁴ and Guido Pupillo¹

¹*icFRC, IPCMS (UMR 7504) and ISIS (UMR 7006),*

Université de Strasbourg and CNRS, 67000 Strasbourg, France

²*Institut für Theoretische Festkörperphysik, JARA-FIT and JARA-HPC,
RWTH Aachen University, 52056 Aachen, Germany*

³*Department of Physics, Harbin Institute of Technology, 150001 Harbin, China*

⁴*Institute for Theoretical Physics, University of Innsbruck,
and IQOQI of the Austrian Academy of Sciences, A-6020 Innsbruck, Austria*

(Dated: April 30, 2022)

Quantum phases of matter are usually characterised by broken symmetries. Identifying physical mechanisms and microscopic Hamiltonians that elude this paradigm is one of the key present challenges in many-body physics. Here, we use quantum Monte-Carlo simulations to show that a Bose metal phase, breaking no symmetries, is realized in simple Hubbard models for bosonic particles on a square lattice complemented by soft-shoulder interactions. The enabling mechanism is provided by cluster formation in the corresponding classical tiling problem. The Bose metal is separated from a superfluid glass by a continuous transition showing non-classical exponents and winding numbers consistent with deconfined quantum criticality. The identification of such cluster mechanism paves the way to the realization of exotic quantum liquids in both natural and synthetic quantum matter that harbors cluster formation.

PACS numbers: 32.80.Ee, 67.80.K-, 05.30.Jp, 61.43.Fs

Many-body bosonic systems exist at low temperature in superfluid or insulating crystalline phases. These archetypical phases are described by finite values of order parameters, reflecting the broken symmetries of the ground state. A remarkable counterexample is provided by Bose metals describing conducting, yet non-superfluid bosons in two dimensions [1–3]. These phases have been suggested as a possible explanation for the strange metal behavior in high-temperature superconductors, and have been theoretically demonstrated in models supporting multi-particle ring-exchange-type interactions [3–5]. However, because of their inherently non-perturbative nature, identifying generic mechanisms and microscopic models that stabilize a Bose metal in realistic Hamiltonians with two-particle interactions has proven challenging.

Here, we show that a whole class of Bose-metal-type phases can be realised in Bose-Hubbard models on square lattices with soft-shoulder interactions, described by the following Hamiltonian

$$\mathcal{H} = -t \sum_{\langle i,j \rangle} (b_i^\dagger b_j + b_j^\dagger b_i) + (V/2) \sum_{i \neq j; r_{ij} \leq r_c} n_i n_j. \quad (1)$$

Here, b_i (b_i^\dagger) are hard-core bosonic annihilation (creation) operators at site i , $n_i = b_i^\dagger b_i$, r_{ij} is the distance between sites i and j , r_c is the cutoff radius of interactions, and t is the tunneling rate on a lattice of spacing a . Such types of interactions have been proposed [6–8], and recently observed [9, 10], in experiments using laser-dressed Rydberg atoms in optical lattices.

The basic mechanism for Bose metal behavior in the aforementioned models is rooted in the emergence of degrees of freedom at strong coupling ($V \gg t$) that are

unrelated to individual particles. These are clusters of particles and holes that are effectively bound by repulsive interactions at high density, with the corresponding classical ground state displaying an extensive degeneracy. In order to show that quantum fluctuations applied to this manifold induce a Bose-metal phase, we employ unbiased large-scale Monte-Carlo simulations. We show that the single particle Green function decays algebraically as a function of distance in the absence of any superfluidity or even crystalline order. This feature and a clear deformation of the Bose surface make our system consistent with the expected behaviour of (d-wave) Bose metals [3].

At weak couplings ($V \simeq t$) this Cluster Bose metal (CBM) is separated from a superglass phase by a second order quantum phase transition, whose critical exponents are at odds with the classical XY criticality in three dimensions [11]. Instead, the statistics of the winding number distribution is found to be in very good agreement with universal predictions [12] for a deconfined quantum critical point (DCP) [13, 14]. The existence of DCPs has been debated in the context of non-Fermi liquid behaviour and quantum phase transitions that may violate the Ginzburg-Landau paradigm [15–21]. Here, we find a sharply different scenario, where the DCP separates an ordered phase from a disordered one [12], and is accompanied by glass behaviour that survives at the critical point.

We start our discussion by illustrating how an extensive ground state degeneracy is realized in the classical limit of Eq. (1). We are interested here in the regime $2\sqrt{2} < r_c/a < 3$, where each particle tries to establish an avoided region of square geometry with total area $16a^2$ (see Fig. 1A). In this regime, for densities $\rho = 1/9$,

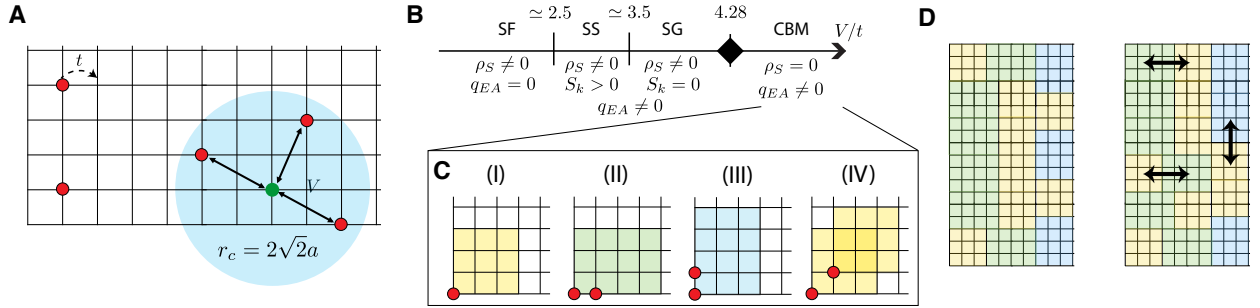


FIG. 1. *Model Hamiltonian and phase diagram.* A) In model Eq. (1), particles are confined to a square lattice with spacing a , and interact via a soft-shoulder potential of range $r_c = 2\sqrt{2}a$ (blue area for the green particle). t is the kinetic energy. B) Sketch of the phase diagram as a function of V/t for density $\rho = 5/36$, including superfluid (SF), supersolid (SS), superglass (SG), and Cluster Bose Metal (CBM) phases. The observables superfluid density ρ_s , static structure factor $S(\mathbf{k})$, the Edward-Anderson parameter \tilde{q}_{EA} , and the momentum distribution $n(k)$ are utilised to distinguish the various phases. The critical point indicated by the black diamond is discussed in Fig. 3. C) In the CBM, the effective dynamics is determined by clusters of type (I-III), which locally minimize the potential energy, while other shapes [e.g., (IV)] are energetically unfavored. D) Examples of possible cluster moves within the cluster phase.

the system can arrange into a state with zero energy. However, this is not possible for higher densities, and the ground state shall be constructed as the solution of a tiling problem of three types of cluster, depicted in Fig. 1C (I-III). Notice that particles now prefer to sit on nearest-neighbors to minimize the potential energy per area, and thus per particle. An exact solution can then be formulated on lattices where $1/6 > \rho > 1/9$ can be decomposed into contributions from both clusters, with total number of particles $N = N_1 + 2 \cdot N_2$ and volume $\mathcal{V} = 9 \cdot N_1 + 12 \cdot N_2$, with N_1 and N_2 the number of clusters made of one (I) or two particles (II-III), respectively. Fixing the ratio $N_2/N_1 = \kappa$, the density reads: $\rho = (1 + 2 \cdot \kappa)/(9 + 12 \cdot \kappa)$. The resulting ground state consists of all permutations of blocks of types I and II-III, and, as in one dimension [22, 23], it displays an exponentially extensive degeneracy. As an example, in the following we focus on the case $\rho = 5/36$, for which, for lattice sizes multiple of four, $N_1/\mathcal{V} = 1/18$ and $N_2/\mathcal{V} = 1/24$ [24], and the classical energy of the configurations is $E/\mathcal{V} = V \cdot N_2/\mathcal{V} = V/24$. For $t > 0$, quantum fluctuations induce an effective dynamics on top of the classical ground state manyfold with a characteristic energy scale $\propto t^2/V$ (see Fig. 1D).

The quantum phase diagram of Eq. (1) is investigated by means of large-scale exact Path Integral Quantum Monte Carlo simulations based on the stochastic Green's function algorithm [25] and is summarised in Fig. 1B. We consider sizes up to $L \times L = 42 \times 42$ lattice sites and temperatures as low as $k_B T = t/(4L)$, with k_B Boltzmann's constant (set to 1 in the following). By increasing the interaction strength V/t , the following succession of phases is obtained: a superfluid, a stripe supersolid, a superglass, and a CBM. The first three phases are well described in literature: The superfluid [$V/t \lesssim 2.5$] and supersolid phases [$2.5 \lesssim V/t \lesssim 3.5$] are lattice analogs

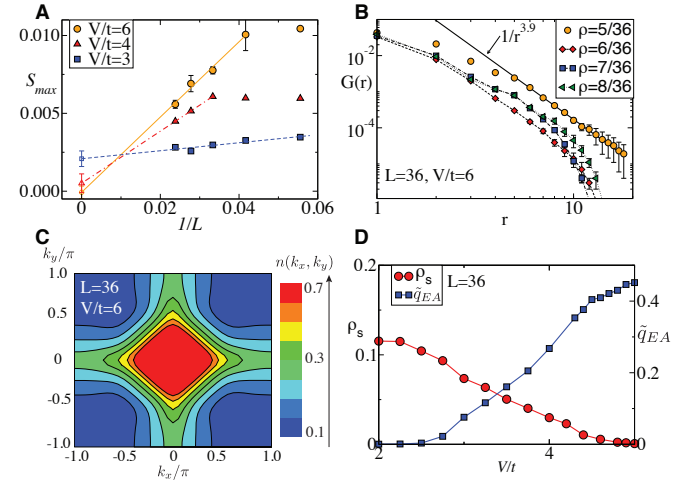


FIG. 2. *Properties of the cluster phase.* A) Finite size scaling of the maximal value of the static structure factor S_{\max} in the SS, SG and CBM phases, with $V/t = 3, 4$ and 6 , respectively ($\beta t = 20$ in all panels). B) Angle averaged Green function $G(r)$ vs distance r for several densities ρ . For $\rho = 5/36$ the decay is algebraic (with exponent increasing as a function of V/t), and exponential otherwise. The continuous line is a fit to the algebraic decay. C) Example of a contour plot of the momentum distribution within the CBM phase, showing pinch points. D) ρ_s (left vertical axis) and \tilde{q}_{EA} (right vertical axis) vs V/t for $L = 36$.

of the corresponding phases in free space [6, 7, 26], characterised by a finite value of the superfluid density ρ_s . In our simulations, we access this quantity via the relation $\rho_s = \langle (W_x^2 + W_y^2) \rangle / (4\beta)$, with W_i the winding number in the i -the direction and $\langle \dots \rangle$ a statistical average. We find that due to the presence of the lattice, however, the crystalline order in the supersolid phase has a stripe-like character, instead of a triangular one, char-

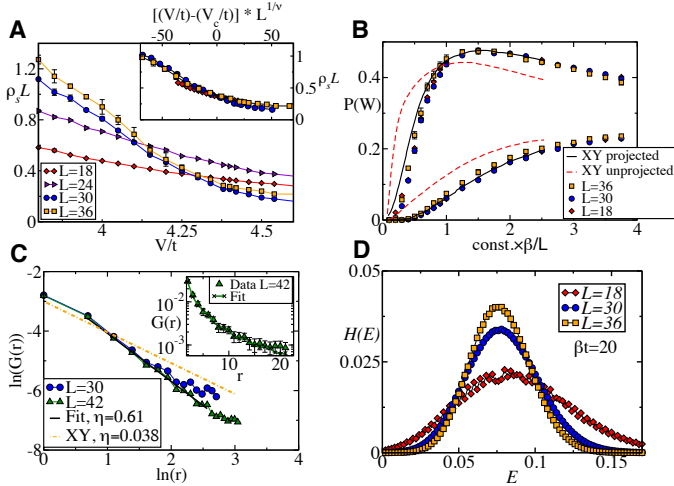


FIG. 3. *Deconfined critical point.* A) $\rho_s L$ vs V/t for several lattice sizes around the SG-CBM transition ($\beta t = 2L$). Inset: data collapse with 3D XY scaling and $\nu = (0.67 \pm 0.05)$ (see text). B) Distribution of winding numbers $P(W)$ as a function of β/L at the SG-CBM transition point. Dashed lines: 3D XY model. Continuous line: universal XY* scaling [12]. C) Green function $G(r)$ vs r at the SG-CBM transition point for $\beta t = 2L$. Continuous line: Best fit of the decay for the largest linear size $L = 42$, implying a non-classical critical exponent $\eta = (0.61 \pm 0.10)$. Dashed line: prediction of the 3D XY model. D) Probability distribution of ground-state energy at the SG-CBM transition point, signaling a continuous phase transition.

acterised by a finite value of the static structure factor $S(\mathbf{k}) = \sum_{i,j} \exp[-i\mathbf{k} \cdot (\mathbf{r}_i - \mathbf{r}_j)] \langle n_i n_j \rangle / L^4$ in the thermodynamics limit, with \mathbf{k} a lattice wave-vector [see example in Fig. 2A, where S_{\max} is the largest value of the peaks in $S(\mathbf{k})$]. For sufficiently strong interactions, the presence of the lattice results in a disordering of the supersolid phase. The ensuing superglass [27–30] is characterised by finite values for ρ_s and for the Edwards-Anderson observable $\tilde{q}_{EA} = q_{EA}/q_{EA}^{\max}$. Here, $q_{EA} = \sum_{i=1}^{L^2} \langle n_i - \rho \rangle^2$ and $q_{EA}^{\max} = L^2 \rho (1 - \rho)$ is its maximum value obtained for a classical situation with no particle delocalization. In the absence of crystalline order, \tilde{q}_{EA} is the well-accepted signature for glassy behavior on a lattice [28, 30], while $S(\mathbf{k}) = 0$ in the thermodynamic limit [30]. A finite value of \tilde{q}_{EA} indicates that in the superglass superfluidity coexists with a sizeable density inhomogeneity in the absence of diagonal order.

The liquid phase present for $V/t \gtrsim 4.3$ defies a description in terms of conventional order parameters: As shown in Fig. 2A-D, its superfluid density and structure factors display no long-range order. Despite this, and in sharp contrast with a quantum glass, we find that correlation functions such as the Green function $G(|i - j|) = \langle b_i b_j^\dagger \rangle$ decay *algebraically* within this phase, indicating the presence of off-diagonal quasi-long-range order. This is accompanied by a clear deformation of the Bose surface, as

depicted in Fig. 2C: the momentum distribution displays pinch points around $(k_x, k_y) = (\pi/2, \pi/2)$, which closely resemble the open Fermi surface structure of d-wave Bose liquids [3]. The specific mechanism underlying this phase can be unfolded by investigating the stability of the quasi-long-range order under perturbations. In Fig. 2B, we show $G(r)$ for various densities doping far away from the cluster limit. For densities not supporting a classical cluster solution, $\rho = 6/36, 7/36, 8/36$, the system behaves as an insulating Bose glass, with finite EA order parameter, but no long-range coherence. This identifies clustering as the backbone ingredient for the stability of the liquid phase, which we then term Cluster Bose Metal. We remark that in this phase quasi-long-range order coexists with glass behavior, which is not surprising as the cluster dynamics in the strong coupling limit proceeds by effective multi-particle updates [see Fig. 1D] that have a distinctly sluggish Monte-Carlo dynamics.

The quantum phase transition between the CBM and superglass phases is characterised in Fig. 3. This transition corresponds to the loss of superfluidity between a (glassy) superfluid and a non-superfluid phase and would naively be expected to belong to the three-dimensional XY universality class [11]. The superfluid density dependence on V/t is depicted in Fig. 3A: except for the case $L = 24$, which shows strong finite-size effects [31], all data can be rescaled such as to collapse on a universal scaling function of $[(V/t) - (V_c/t)] * L^{(1/\nu)}$. Assuming a dynamical critical exponent $z = 1$, we extract $V_c/t = 4.28 \pm 0.01$ and with $\nu \simeq 0.67 \pm 0.05$, thus compatible with an XY scaling [32]. However, the critical exponent $\eta \simeq 0.61 \pm 0.10$, extracted from the real-space decay of the Green function $G(r) \sim 1/r^{1+\eta}$ shown in Fig. 3C, displays a clear departure from its expected classical value 0.038 [11]. This highly non-classical value points toward the possibility of a deconfined critical point, e.g., a quantum critical point whose low-energy description is given in terms of a deconfined gauge theory. In order to confirm this scenario, we monitor the full distribution of winding numbers as quantified by the probabilities $P(W)$ of observing a given winding. As proposed in Refs. [12], as a consequence of the universality of the winding-number variance $\langle W^2 \rangle$, the latter probabilities are expected to be universal functions of $L/v\beta$, with v a non-universal velocity. Crucially, these probabilities contain direct information on the existence of fractionalized excitations and the emergence of \mathbb{Z}_2 gauge fields at the critical point.

Figure 3B shows example results for $P(W)$ as a function of β/L at $(V/t)_c$ for our model Eq. (1), compared to those of Ref. [12] for the conventional XY model on the square lattice. The fitting of all scaling functions uses only a single adjustable parameter, the non-universal velocity ratio v_{XY}/v . The figure shows that for increasing values of β/L (i.e., for decreasing temperature T) our results significantly differ from those of the conventional

XY model, and are compatible with the projected XY scaling expected for DCP. We note that the exponent η observed in our simulations is smaller than expectations based on XY* criticality: this might be due to the fact that, at the transition point, the system dynamics is still glassy, as signalled by a finite \tilde{q}_{EA} , which can affect the dynamics of the emergent degrees of freedom.

We note that unlike previous proposals [15–19, 33], here the DCP separates an ordered and a disordered phase (similar to Ref. [12]) and thus is not immediately related to the violation of the Ginzburg-Landau scenario for phase transitions. The probability distribution of energies close to the transition point for different system sizes [see Fig. 3D] displays here a single peak that grows with the system size, consistent with a continuous transition as discussed above.

The simplicity of the model discussed here paves the way to the observation of Bose metal and deconfined criticality in various microscopic systems, including laser-dressed Rydberg atoms in optical lattices [6–8], where the realization of soft-shoulder potentials has recently been reported [9, 10]. Extending this work to fermionic systems with variable interaction range supporting clusters could shed light on the microscopic mechanism of non-Fermi liquid behaviour in two-dimensional extended Fermi-Hubbard models.

We acknowledge useful discussion with A. Kuklov, W. Lechner, M. Mattioli, N. Prokof'ev and S. Wessel. Work in Strasbourg was supported by the ERC St-Grant ColDSIM (No. 307688), with additional funding from Rysq and ANR-FWF grant BLUESHIELD. Work in Innsbruck was supported in part by the ERC Synergy Grant UQUAM, SIQS, and the SFB FoQuS (FWF Project No. F4016-N23). T. Y. was also supported by the National Natural Science Foundation of China (No. 11504067).

- [6] N. Henkel, R. Nath and T. Pohl, *Phys. Rev. Lett.* **104**, 195302 (2010).
- [7] F. Cinti, P. Jain, M. Boninsegni, A. Micheli, P. Zoller, and G. Pupillo, *Phys. Rev. Lett.* **105**, 135301 (2010).
- [8] J. Honer, H. Weimer, T. Pfau, and H. P. Büchler, *Phys. Rev. Lett.* **105**, 160404 (2010).
- [9] Y. Y. Jau, A. M. Hankin, T. Keating, I. H. Deutsch, and G. W. Biedermann, *Nature Physics* **12**, 71–74 (2016).
- [10] J. Zeiher *et al.*, arXiv.1602.06313.
- [11] A. Pelissetto and E. Vicari, *Phys. Rep.* **368**, 549 2002 .
- [12] S. V. Isakov, R. G. Melko, and M. B. Hastings, *Science* **335**, 193 (2012).
- [13] T. Senthil, A. Vishwanath, L. Balents, S. Sachdev, and M. P. A. Fisher, *Science* **303**, 1490 (2004)
- [14] T. Senthil, L. Balents, S. Sachdev, A. Vishwanath, and M. P. A. Fisher, *Phys. Rev. B* **70**, 144407 (2004).
- [15] A. B. Kuklov, M. Matsumoto, N. V. Prokof'ev, B. V. Svistunov, and M. Troyer, *Phys. Rev. Lett.* **101**, 050405 (2008).
- [16] Kun Chen, Yuan Huang, Youjin Deng, A. B. Kuklov, N. V. Prokof'ev, and B. V. Svistunov, *Phys. Rev. Lett.* **110**, 185701 (2013).
- [17] A. W. Sandvik, *Phys. Rev. Lett.* **98**, 227202 (2007).
- [18] F.-J. Jiang, M. Nyfeler, S. Chandrasekharan, and U.-J. Wiese, *J. Stat. Mech.* (2008) P02009.
- [19] A. W. Sandvik, *Phys. Rev. Lett.* **104**, 177201 (2010).
- [20] K. Harada *et al.*, *Phys. Rev. B* **88**, 220408 (2013R).
- [21] S. Pujari, K. Damle, and F. Alet, *Phys. Rev. Lett.* **111**, 087203 (2013).
- [22] M. Mattioli, M. Dalmonte, W. Lechner, and G. Pupillo, *Phys. Rev. Lett.* **111**, 165302 (2013).
- [23] M. Dalmonte *et al.*, *Phys. Rev. B* **92**, 045106 (2015).
- [24] We note that for some of the system sizes considered here, where $\text{mod}_4 L = 2$, there are multiple cluster configurations attainable with different densities: in this case, we sample both cases in the QMC simulations.
- [25] V. Rousseau, *Phys. Rev. E* **77**, 056705 (2008).
- [26] F. Cinti, T. Macrì, W. Lechner, G. Pupillo and T. Pohl, *Nature Comm.* **5**, 3235 (2014).
- [27] M. Boninsegni, N. Prokof'ev, and B. Svistunov, *Phys. Rev. Lett.* **96**, 105301 (2006).
- [28] G. Carleo, M. Tarzia, and F. Zamponi, *Phys. Rev. Lett.* **103**, 215302 (2009).
- [29] K.-M. Tam, S. Geraedts, S. Inglis, M. J. P. Gingras, and R. G. Melko, *Phys. Rev. Lett.* **104**, 215301 (2010).
- [30] A. Angelone, F. Mezzacapo, and G. Pupillo, *Phys. Rev. Lett.* **116**, 135303 (2016).
- [31] L=24 it is the smallest size available where the cluster can re-arrange in parallel wires.
- [32] M. Campostrini, M. Hasenbusch, A. Pelissetto and E. Vicari, *Phys. Rev. B* **74**, 144506 (2006).
- [33] Anatoly Kuklov, Nikolay Prokof'ev, and Boris Svistunov, *Phys. Rev. Lett.* **93**, 230402 (2004).

- [1] M. V. Feigelman, V. B. Geshkenbein, L. B. Ioffe and A. I. Larkin, *Phys. Rev. B* **48**, 16641 (1993).
- [2] P. Phillips and D. Dalidovich, *Science* **302**, 243 (2003).
- [3] O. I. Motrunich and M. P. A. Fisher, *Phys. Rev. B* **75**, 235116 (2007).
- [4] H.-C. Jiang *et al.*, *Nature* **493**, 39 (2013).
- [5] M. S. Block, D.N. Sheng, O.I. Motrunich and M. P. A. Fisher, *Phys. Rev. Lett.* **106**, 157202 (2011).